

Ground-motion prediction from tremor

Annemarie S. Baltay¹ and Gregory C. Beroza²

Received 28 October 2013; revised 3 December 2013; accepted 6 December 2013; published 26 December 2013.

[1] The widespread occurrence of tremor, coupled with its frequency content and location, provides an exceptional opportunity to test and improve strong ground-motion attenuation relations for subduction zones. We characterize the amplitude of thousands of individual 5 min tremor events in Cascadia during three episodic tremor and slip events to constrain the distance decay of peak ground acceleration (PGA) and peak ground velocity (PGV). We determine the anelastic attenuation parameter for ground-motion prediction equations (GMPEs) to a distance of 150 km, which is sufficient to place important constraints on ground-motion decay. Tremor PGA and PGV show a distance decay that is similar to subduction-zone-specific GMPEs developed from both data and simulations; however, the massive amount of data present in the tremor observations should allow us to refine distance-amplitude attenuation relationships for use in hazard maps, and to search for regional variations and intrasubduction zone differences in ground-motion attenuation. **Citation:** Baltay, A. S., and G. C. Beroza (2013), Ground-motion prediction from tremor, *Geophys. Res. Lett.*, 40, 6340–6345, doi:10.1002/2013GL058506.

1. Introduction

[2] The Cascadia subduction zone is known to produce large megathrust earthquakes of magnitude up to ~9, accompanied by tsunami, which are expected to recur and will likely cause widespread strong ground shaking and damage along the populous corridor from Portland through Seattle to Vancouver [Atwater, 1987; Atwater *et al.*, 1995; Satake *et al.*, 1996]. This threat motivates the development of updated hazard maps for this region, which require accurate ground-motion prediction equations (GMPEs) [Petersen *et al.*, 2008]. In practice, GMPEs are determined empirically with earthquake data recorded at many stations; however, in some areas of high earthquake hazard, such as Cascadia, the data set of recorded earthquakes for ground-motion prediction is sparse [e.g., Atkinson and Boore, 1997].

[3] Tectonic tremor in Cascadia presents an exceptional opportunity to test and improve strong ground-motion attenuation relations. Tremor consists of many bursts of small amplitude seismic signal, thousands of which are recorded during each episodic tremor and slip (ETS) event [Rogers

and Dragert, 2003; Wech and Creager, 2008]. Tectonic tremor has been observed to occur on the subducting plate interface [La Rocca *et al.*, 2009; Brown *et al.*, 2009; Rubinstein *et al.*, 2010; Beroza and Ide, 2011], likely near the downdip limit of rupture of future large megathrust earthquakes, the area that is expected to control high-frequency shaking [Ide *et al.*, 2011; Lay *et al.*, 2012]. Tremor is well recorded seismically on the high-sensitivity, high signal-to-noise-ratio (SNR) borehole stations of the Plate Boundary Observatory (PBO), which is distributed throughout Cascadia. Finally, tremor is radiated most strongly in the 1–10 Hz frequency band, which closely matches frequencies of interest in engineering seismology and strong ground-motion prediction [Rogers and Dragert, 2003; Jennings, 2003]. Therefore, tremor is well situated for developing improved GMPEs.

2. Tectonic Tremor as Ground-Motion Data

[4] We consider tremor occurring during the August 2010, August 2011, and September 2012 ETS episodes, during which over 45,000 5 min tremor windows are defined and located beneath Vancouver Island, the Olympic Peninsula, southern Washington, and Northern Oregon (Figure 1) [Wech and Creager, 2008; <http://www.pnsn.org/tremor>]. We consider each 5 min window a discrete tremor “event” and determine the PGA and PGV from each record, as well as the hypocentral distance to stations in the PBO network, assuming, for simplicity, a constant source depth of 30 km. Synthetic studies indicate that the final value of anelastic attenuation is not very dependent on this assumed depth (S. Yabe, pers. communication, 2013).

[5] For each station in the PBO borehole seismic network, we obtain continuously recorded data through IRIS SOD with instrument response removed [Owens *et al.*, 2004] and geometrically average the two horizontal components. Because tectonic tremor is most pronounced from 1 to 10 Hz, we band pass the data in that range with a two-pass, four-pole Butterworth filter. For each 5 min event window, the data are differentiated to velocity and again to acceleration, and the peak values within the time window taken as the peak ground velocity (PGV) and acceleration (PGA). Events with the same timing but different locations are excluded, without a concrete way to determine the correct epicentral distance. Events starting just before midnight or ending just after are discarded due to data continuity; all of these discarded events account for a small fraction of the available data.

[6] The distance-amplitude decay of each station is visually inspected (e.g., Figure 2a), and several stations are discarded due to noise contamination at some point during the ETS events, with stations used shown by triangles (Figure 1). Due to the considerable amount of data in our study (over 45,000 events recorded at 13 stations with three components), it is impossible to inspect the quality of individual records visually.

Additional supporting information may be found in the online version of this article.

¹Earthquake Science Center, USGS Menlo Park, Menlo Park, California, USA.

²Department of Geophysics, Stanford University, Stanford, California, USA.

Corresponding author: A. S. Baltay, Earthquake Science Center, USGS Menlo Park, Menlo Park, CA 94025, USA. (abaltay@usgs.gov)

©2013. American Geophysical Union. All Rights Reserved.
0094-8276/13/10.1002/2013GL058506

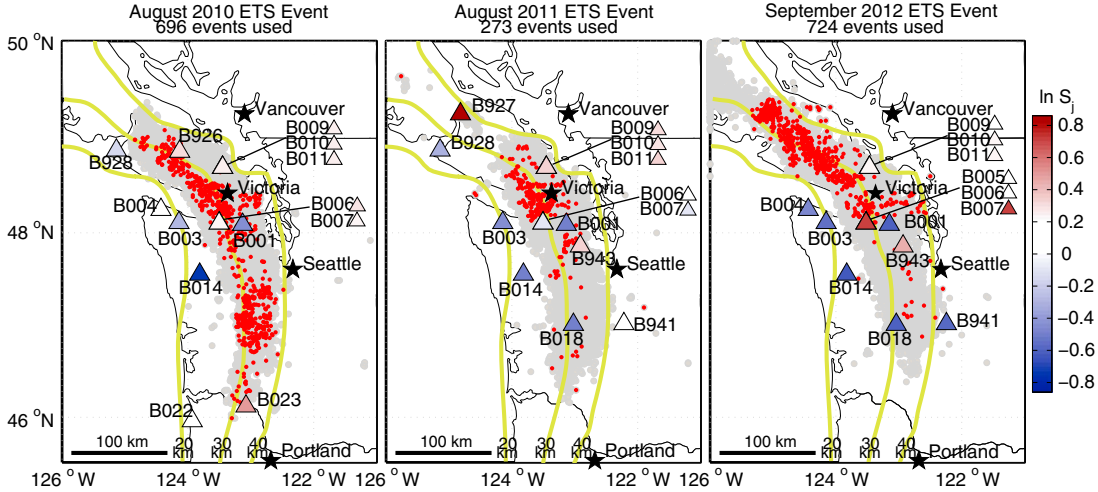


Figure 1. Locations of 5 min tremor events used in the inversion (red dots) overlaid on all available data (grey dots). Yellow lines show the plate interface [Audet *et al.*, 2010]. Triangles show stations used, with color indicating the mean site/station term (S_j). Stations B009, B010, and B011 are within 250 m of each other, located within the triangle on the map, with individual stations shown in color following the connecting line; the same applies to B005, B006, and B007.

Some contamination is likely present in the data set but should be overcome by the amount of signal available.

[7] Along with the peak values, we test other metrics of amplitude, i.e., mean and RMS, within each 5 min tremor event. We find that for various window lengths between 3 and 30 s, both the RMS and mean amplitudes display very similar distance decay behavior to the peak values, albeit with different absolute amplitudes. That these different metrics of amplitude decay comparably with distance supports the notion that the amplitude-distance decay estimated is robust.

3. Differential Amplitude Inversion to Find Attenuation and Magnitude Term

[8] Ground-motion prediction equations (GMPEs) describe the relationship of ground-motion amplitude, typically PGA, PGV, or spectral acceleration (SA), to distance and magnitude, as well as other predictive parameters, such as

style of faulting, size of fault plane, distance from surface projection, or site response [Abrahamson *et al.*, 2013]. We consider a simplistic GMPE, when parameters other than magnitude and distance are unknown:

$$A_{ij} = A_{io} \exp\left(\frac{-\pi R_{ij} f}{Q\beta}\right) \frac{1}{R_{ij}} S_j \quad (1)$$

[9] The amplitude of ground motion from an earthquake, i , recorded at station j with hypocentral distance R_{ij} and frequency f , can be expressed as the initial amplitude (at $R=0$) of that earthquake, A_{io} , combined with geometrical spreading, $1/R$; anelastic attenuation, with Q the quality factor; a site term for the particular station, S_j ; and β , the shear wave velocity. In practice, the initial source amplitude A_o is a function of earthquake magnitude. In this study, we fix the geometrical spreading as $1/R$ to avoid complications with the trade-off between this term and the attenuation term, although for GMPE development, a coefficient other than -1 (i.e., $1/R$) is allowed.

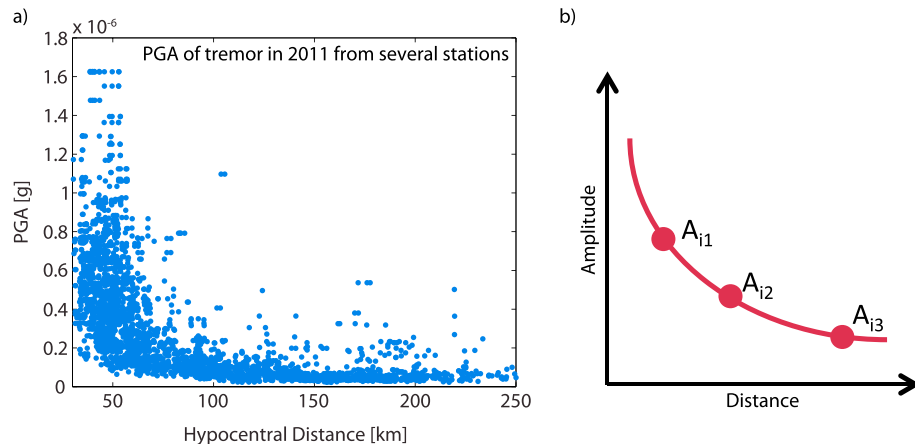


Figure 2. (a) Distance decay of PGA from tremor events in 2011 recorded at several stations. A clear $1/R$ decay trend is apparent, despite mixed event magnitudes. (b) Schematic representation of (a) for event i at stations 1, 2, and 3. By comparing amplitudes of the same event at different distances (stations), magnitude information is not required.

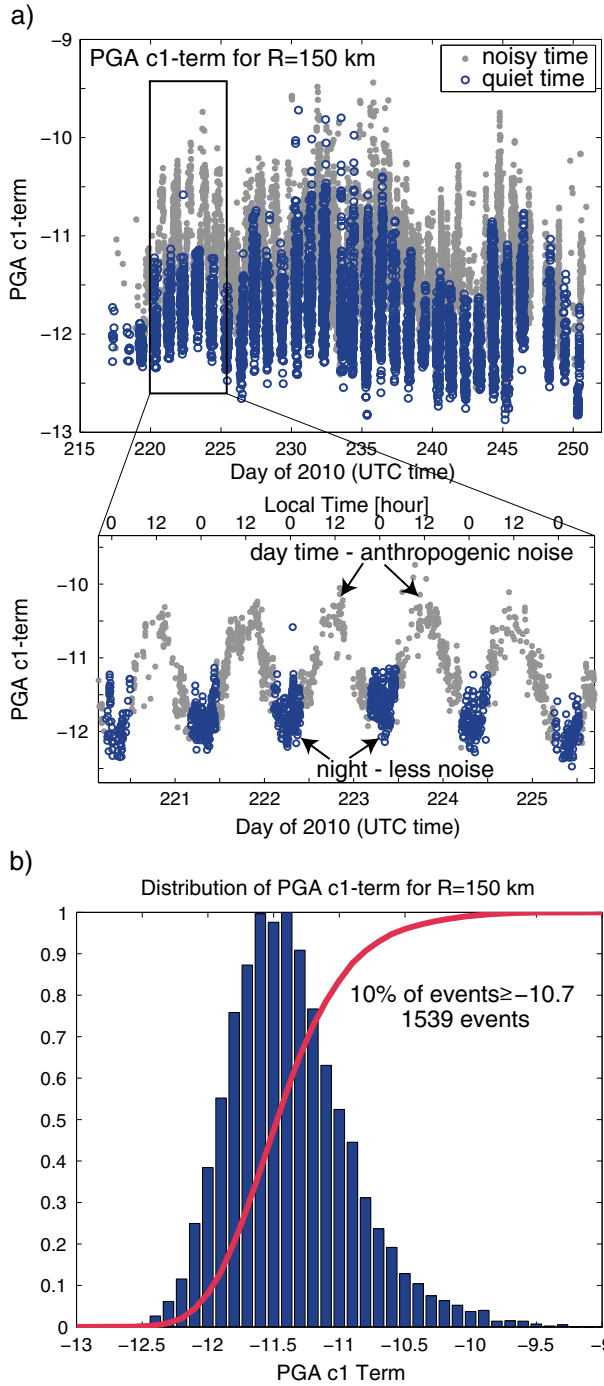


Figure 3. Distribution of PGA $c1$ -term, representative of the magnitude of the individual tremor events. (a) Variation of $c1$ with time throughout the 2010 ETS event. Zoom-in shows the oscillatory behavior of the $c1$, artificially amplified during the day due to anthropogenic noise. Only 7 h of data during the night are used for the analysis. (b) Distribution of $c1$ from nighttime data. To increase the data quality, the largest 10% (1539) of tremor events are used.

[10] Parameterizing equation (1) in natural-log form and temporarily ignoring the station term:

$$\ln A_{ij} = c1_i - c2R_{ij} - \ln R_{ij} \quad (2)$$

where $c1$ is common to all recordings of any given earthquake, i , describing the initial amplitude and dependent on

magnitude, typically with a linear or even quadratic dependency [Abrahamson *et al.*, 2013], and $c2$ describes the apparent anelastic attenuation parameter, $c2 = \pi f/Q\beta$. For our study, we do not explicitly consider frequency, as we model only PGA and PGV, which do not have a defined frequency, within the 1–10 Hz band-pass filtered tremor signal.

[11] We use the observed amplitude decay with distance to estimate the anelastic attenuation parameter from the tremor PGA and PGV. The larger tremor bursts can easily be seen by eye across the PBO network to distances greater than 100 km (Figure S1) despite their very small amplitudes (PGA of $\sim 1\text{--}2 \times 10^{-6}$ g, compared with typical felt ground motions of a few percent of gravity [Wald *et al.*, 1999]). A clear amplitude decay to a distance of about 150 km can be seen as expected following equation (1) (Figure 2a). Background noise in Cascadia has a peak at about 3×10^{-7} m/s² in the frequency band we consider, i.e., 1–10 Hz, as observed at a PBO borehole station on a nontremor day (Figure S2). Rubinstein *et al.* [2007] showed that tremor in Cascadia recorded at a close station is at least an order of magnitude larger than the local noise for frequencies in the 2–10 Hz range (at 1 Hz, the signal is $\sim 4\times$ greater than the noise). When the tremor amplitude recorded at a distant station is equal to or less than the background noise level, our peak ground-motion measure simply reflects noise. This occurs at a distance of ~ 150 km. At closer stations, the PGA signal is primarily attributable to tremor, as the noise level is below the signal level.

[12] Our ground-motion data set of PGA and PGV measurements from 5 min tremor events does not contain a priori magnitude for any events. Rather than estimate magnitude independently, we use differential ground-motion amplitudes from single events recorded at different stations to determine the ground-motion attenuation terms, shown schematically in Figure 2b. The amplitude (PGA or PGV) from event i at station 1 (A_{i1}) and amplitude from event i at station 2 (A_{i2}) can be written as $\ln A_{i1} = c1_i - c2R_{i1} - \ln R_{i1}$ and $\ln A_{i2} = c1_i - c2R_{i2} - \ln R_{i2}$, respectively, following equation (2). Subtracting the two expressions cancels the common event term, $c1_i$, leaving only differences in ground-motion amplitudes and differences in distances.

$$\frac{(\ln A_{i1} - \ln A_{i2}) + (\ln R_{i1} - \ln R_{i2})}{(R_{i2} - R_{i1})} = c2 \quad (3)$$

[13] First, the best fitting, least squares (L2) solution for $c2$ for every station pair for each event is determined. Due to instabilities that arise when stations are closely clustered, as is the case with B009, B010, and B011, as well as B005, B006, and B007, from the denominator of equation (3), we exclude station pairs that are within 1 km of each other.

[14] Next, after finding an estimate of $c2$ from equation (3), we back-substitute to recover $c1$ for each event, i , taken as the mean over all station measurements recording that event:

$$c1_i = \frac{1}{M} \sum_{j=1}^M \ln A_{ij} + \ln R_{ij} + c2R_{ij} \quad (4)$$

[15] Third, we determine an average station or site term, S_j , assuming that all events recorded at the same station, j , will be affected by the same amplification or attenuation, due to near-site conditions:

$$\ln S_j = \frac{1}{N} \sum_{i=1}^N \ln A_{ij} - c1_i + \ln R_{ij} + c2R_{ij} \quad (5)$$

Table 1. Values of c_2 (Anelastic Attenuation) for PGA and PGV, for the Whole Data Set Together Compared to Values for Each Year Separately, With Preferred Values in Bold

	PGA				PGV			
	All	2010	2011	2012	all	2010	2011	2012
Median	0.00647	0.00644	0.00666	0.00645	0.00471	0.00467	0.00480	0.00470
Mean	0.00638	0.00653	0.00620	0.00632	0.00457	0.00472	0.00439	0.00452
Std. err	5.552e-5	8.954e-5	1.292e-4	8.436e-5	4.494e-5	7.087e-5	1.114e-4	6.746e-5

with c_1 and c_2 from the previous steps. The site/station terms, S_j , are shown in Figure 1 by the color of the station triangle. Although S_j for each station is considered separately for each ETS event (2010, 2011, and 2012), stations that are used in multiple years show similar values.

[16] Finally, the ultimate c_2 depends on S_j for each station and c_1 for each event:

$$c_2 = \frac{\ln A_{ij} - \ln S_j - c_1 i + \ln R_{ij}}{-R_{ij}} \quad (6)$$

[17] In an initial analysis, we use all of the data in equations (3) and (4) to find c_2 and then c_1 . These initial values of c_1 are used to isolate events with the largest relative amplitudes and high SNR (Figure 3). Nominal values for c_1 range from -13 to -9 , reinforcing the fact that the c_1 term is a function of magnitude, but is not absolute magnitude: estimates of duration-based magnitude for 5 min of tremor in Cascadia are $\sim M_w 3$ [Aguilar *et al.*, 2009]; amplitude-based magnitudes for low-frequency earthquakes within tremor in Japan are in the range of $M 0$ to $M 1.5$ [Shelly *et al.*, 2006].

[18] There is a strong dependence of c_1 on time of day: tremor amplitudes appear much larger, by two orders of magnitude, during the day than at night (Figure 3a). A 24 h periodic modulation has previously been observed in Cascadia tremor [Rubinstein *et al.*, 2008]. In our data, two peaks are discernable each day (e.g., just before day 222), possibly indicating a morning and evening rush hour. This is likely simply a detection issue, indicating that local anthropogenic noise from traffic has higher amplitudes than the tectonic tremor; thus, data recorded during the day are contaminated.

[19] To avoid anthropogenic noise contamination, we consider only data recorded during the quieter 7 h at night. We further restrict the data to the largest 10% of these events (red dots in Figure 1; Figure 3b). Our remaining 1539 tremor events, recorded at as many as 13 stations, show much clearer distance-amplitude decay trends compared to the original, nonquality-controlled data, yet still represent a wealth of data with which to constrain the anelastic attenuation parameter.

[20] With the winnowed data set, we repeat the analysis from the beginning to estimate the final anelastic attenuation parameter, c_2 , from equation (6). The distribution of c_2 from all event-station pairs follows the Laplace probability density function (equation (7); Figure S3):

$$F(x|\mu, b) = \frac{1}{2b} \exp\left(-\frac{|x - \mu|}{b}\right) \quad (7)$$

with μ the location parameter, or sample median, b the scale parameter, and $\sqrt{2}b$ the standard deviation. The Laplace distribution is expressed in terms of the absolute difference from the mean. Thus, L1-norm minimization gives the maximum likelihood estimator, which is the sample median. The Laplace distribution describes the ratio of two log-normally

distributed random variables, similar to the relationship for c_2 from equation (6).

[21] An ideal Laplace pdf with μ and b the sample median and standard deviation fits the data well (Figure S3), indicating that the sample median is the best estimator for data mean. By comparing the values for the different years, we confirm that the median, rather than the mean, gives a more stable estimate between different subsets of the data (year 2010, 2011, and 2012) (Table 1). The c_2 values for each year are similar for either case. A nonparametric boxplot of c_2 values from each year of tremor data indicates that the distributions are similar; the overlap of notches in the boxes implies that the median values from year to year do not differ at the 95% confidence level (Figure S4).

[22] The final value for c_2 for PGA and PGV is taken from the median value over all the years. Due to the large sample size and Laplace distribution of the data, the standard error of the median is very small. Figure 4 shows the PGA and PGV data, A_{ij} , for each event and station, adjusted by each respective site, S_j , and source, c_1 , term plotted against distance with the best fit c_2 . Residuals are evenly distributed around 0, indicating that the c_2 value is a good descriptor for the data at all distances considered (Figure 4c). A misfit of the data may indicate that a different geometrical spreading relationship is necessary, but we find no strong evidence to support this.

[23] Throughout the analysis, we have restricted the data to records within 150 km of the tremor hypocenters. We explore the effect of the distance threshold on the results (Figure S5). At closer distances, less than 80 km, there are few data points with which to constrain the attenuation parameter, and hence c_2 is not stable. At greater distance, when the tremor signal decays below the noise level, PGA and PGV data points reflect noise, and the data set levels off at the background floor (Figure 2). Then, c_2 becomes unstable, reflecting a fit to the noise, rather than the data (Figure S5). Synthetic studies (S. Yabe, pers. communication, 2013) indicate that the true value of the anelastic attenuation is found where the result stabilizes, with respect to distance. At closer distances, the anelastic attenuation parameter is unstable due to fewer data points, while at greater distances, the inclusion of noise causes the attenuation parameter to decrease. Our result is very stable at distances near 150 km.

[24] We compare our results to the Atkinson and Boore [1997] study in Cascadia, which coupled stochastic simulations and earthquake records from magnitudes 4 to 8.2. For PGA, we find a remarkably similar value for the attenuation parameter, 0.00647 as compared to 0.00645, ostensibly due to the high-frequency nature of PGA, such that the source characteristics are not important. For PGV, our $c_2=0.00471$ is larger than $c_2=0.00253$ of Atkinson and Boore [1997], implying greater attenuation. This discrepancy is likely due to the higher frequency of tremor PGV as compared to that of the considered earthquakes. PGV for earthquakes should be at

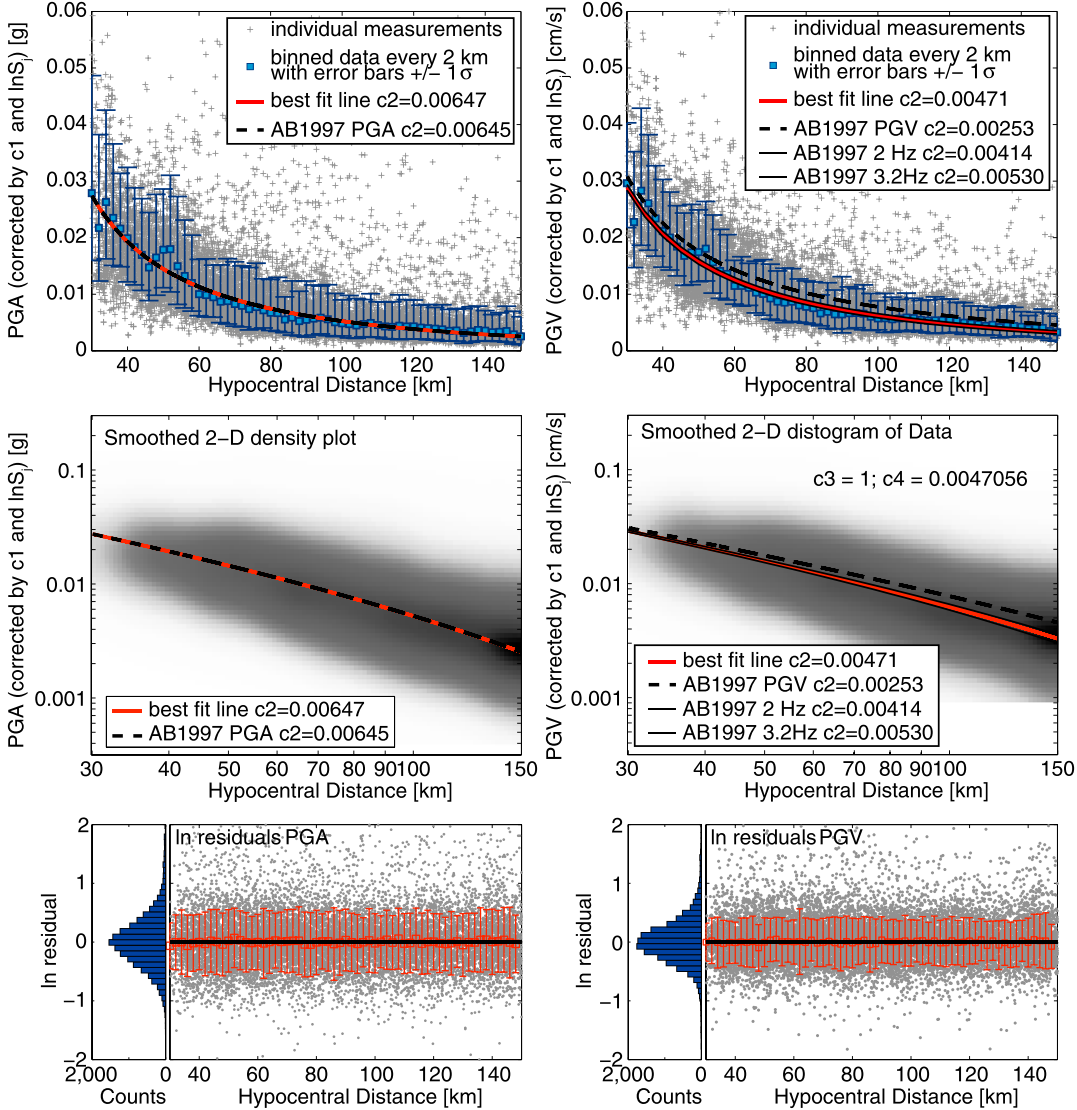


Figure 4. (Left) PGA and (right) PGV for the reduced, final, data set, adjusted for c_1 and site term, S_j . Our best fitting (median) c_2 (red lines) shown in comparison to Atkinson and Boore [1997]. (a) Individual PGA, PGV recordings (crosses) with 2 km distance bins (squares) and error bars. (b) Density plot of the same PGA, PGV recordings, on a log-log plot. (c) Natural-log residuals between individual data points and the best fit model. The residuals show no distance bias and are normally distributed (histogram).

frequencies near the corner frequency, at or below ~ 1 Hz for the moderate to large earthquakes used in Atkinson and Boore [1997], while tremor velocity spectra have a broad peak near $2 - 4$ Hz [Brown *et al.*, 2013]. We expect PGV attenuation values to correspond to spectral acceleration attenuation values at the frequency where PGV occurs. The Atkinson and Boore [1997] study finds a PGV attenuation of $c_2 = 0.00253$, and attenuation values of $c_2 = 0.00207$ and $c_2 = 0.00276$ for spectral acceleration at the frequencies of 0.5 Hz and 0.8 Hz, respectively, the expected average corner frequency for the earthquakes considered. Our tremor PGV attenuation parameter, $c_2 = 0.00471$, falls between the spectral acceleration attenuation values of Atkinson and Boore [1997] at frequencies of 2 Hz ($c_2 = 0.00414$) and 3.2 Hz ($c_2 = 0.00530$), consistent with a peak in the tremor velocity spectrum near $2 - 4$ Hz [Brown *et al.*, 2013]. The similarity of the results implies that our method can be used to estimate the c_2 anelastic attenuation parameter.

4. Implications and Conclusions

[25] In this proof-of-concept study, we show that tectonic tremor signal, despite its low amplitude and lack of absolute magnitude information, can be used to determine the anelastic attenuation parameter, c_2 , for PGA and PGV, for application to GMPEs. We find that a hypocentral distance of 150 km is most stable for capturing the attenuation, and the values determined here are similar to Cascadia-specific GMPEs [Atkinson and Boore, 1997]. The wealth of tremor data allows us to determine more precisely the anelastic attenuation parameter; due to the limited frequency band of tectonic tremor and the frequency dependence of the PGV, the relationship between attenuation as determined here and that from regular earthquakes needs to be clarified.

[26] If tectonic tremor can be used for GMPE development or validation, the spatial resolution of hazard maps could be greatly increased. This technique can be applied to other

high-hazard areas where tremor is well recorded, such as the subduction zones of Japan, Alaska, or Mexico. Due to the spatial density of both tremor events and stations in many of these areas, and the high precision of this method, regional variations could be determined, such as depth-dependent changes in amplification, differences in whole path attenuation as signals travel either along the subducting plate or perpendicular to it, or for paths of great interest, such as that from the subducting plate to metropolitan Seattle.

[27] This method could also be adapted further for use in GMPEs. By filtering the initial data in narrower frequency bands between 1 and 10 Hz, the dependence on various frequencies could be examined. These attenuation parameters could be used in GMPEs for specific frequencies of spectral acceleration (SA), rather than simply PGA and PGV, which are more sensitive to the source characteristics. As well, we have kept the geometrical spreading coefficient to -1 (i.e., $1/R$), while in practice, this coefficient may differ from -1 , and could be fit simultaneously, albeit with direct trade-off to the attenuation parameter. Finally, we have also shown that the effect of a site term is robust, and this information could be used for determination of relative site factors in GMPEs. The amplitude information from tectonic tremor represents a wealth of information that has substantial untapped potential for ground-motion prediction.

[28] **Acknowledgments.** The authors are extremely grateful to Sirada Asawachaisujja for initial analysis of Cascadia data while a SURGE intern at Stanford in 2012; to Suguru Yabe and Satoshi Ide for helpful discussion and synthetic study results; to Justin Rubinstein, Art Frankel, Adrien Oth, and an anonymous reviewer for thorough reviews. A. S. Baltay is supported by a Mendenhall Fellowship at the USGS and was supported by Pacific Gas and Electric during 2012. This research was also supported by SCEC (NSF Cooperative Agreement EAR-0529922, USGS Cooperative Agreement 07HQAG0008). SCEC paper number 1795.

[29] The Editor thanks Adrien Oth and an anonymous reviewer for their assistance in evaluating this paper.

References

- Abrahamson, N. A., W. J. Silva, and R. Kamai (2013), Update of the AS08 Ground-Motion Prediction Equations Based on the NGA-West2 Data Set, *PEER Report No. 2013/04*, Pacific Earthquake Engineering Research Center, University of California, Berkeley, CA.
- Aguiar, A. C., T. I. Melbourne, and C. W. Scrivner (2009), Moment release rate of Cascadia tremor constrained by GPS, *J. Geophys. Res.*, **114**, B00A05, doi:10.1029/2008JB005909.
- Atkinson, G. M., and D. M. Boore (1997), Stochastic point-source modeling of ground motions in the Cascadia region, *Seismol. Res. Lett.*, **68**.
- Atwater, B. F. (1987), Evidence for great Holocene earthquakes along the outer coast of Washington State, *Science*, **236**, 942–944, doi:10.1126/science.236.4804.942.
- Atwater, B. F., et al. (1995), Summary of Coastal Geologic Evidence for Past Great Earthquakes at the Cascadia Subduction Zone, *Earthq. Spectra*, **11**(1), 1–18.
- Audet, P., M. G. Bostock, D. C. Boyarko, M. R. Brudzinski, and R. M. Allen (2010), Slab morphology in the Cascadia fore arc and its relation to episodic tremor and slip, *J. Geophys. Res.*, **115**, B00A16, doi:10.1029/2008JB006053.
- Beroza, G. C., and S. Ide (2011), Slow earthquakes and nonvolcanic tremor, *Annu. Rev. Planet. Earth Sci.*, **39**, 271–296.
- Brown, J. R., G. C. Beroza, S. Ide, K. Ohta, D. R. Shelly, S. Y. Schwartz, W. Rabbel, M. Thorwart, and H. Kao (2009), Deep low-frequency earthquakes in tremor localize to the plate interface in multiple subduction zones, *Geophys. Res. Lett.*, **36**, L19306, doi:10.1029/2009GL04002.
- Brown, J. R., S. G. Prejean, G. C. Beroza, J. S. Gomberg, and P. J. Haussler (2013), Deep low-frequency earthquakes in tectonic tremor along the Alaska-Aleutian subduction zone, *J. Geophys. Res. Solid Earth*, **118**, 1079–1090, doi:10.1029/2012JB009459.
- Ide, S., A. S. Baltay, and G. C. Beroza (2011), Shallow dynamic overshoot and energetic deep rupture of the 2011 $M_w 9.0$ Tohoku-Oki earthquake, *Science*, **332**(6036), 1426–1429, doi:10.1126/science.1207020.
- Jennings, P. C. (2003), An introduction to the earthquake response of structures, in *International Handbook of Earthquake and Engineering Seismology*, vol. 81B, edited by W. H. K. Lee et al., Academic Press, Amsterdam, pp. 1097–1125.
- La Rocca, M., K. C. Creager, D. Galluzzo, S. Malone, J. E. Vidale, J. R. Sweet, and A. G. Wech (2009), Cascadia tremor located near plate interface constrained by S minus P wave times, *Science*, **323**, 620–623, doi:10.1126/science.1167112.
- Lay, T., H. Kanamori, C. J. Ammon, K. D. Koper, A. R. Hutko, L. Ye, H. Yue, and T. M. Rushing (2012), Depth-varying rupture properties of subduction zone megathrust faults, *J. Geophys. Res.*, **117**, B04311, doi:10.1029/2011JB009133.
- Owens, T. J., H. P. Crotwell, C. Groves, and P. Oliver-Paul (2004), SOD: Standing Order for Data, *Seismol. Res. Lett.*, **75**, 515–520.
- Petersen, M. D., et al. 2008, Documentation for the 2008 Update of the United States National Seismic Hazard Maps: U.S. Geological Survey Open-File Report 2008-1128, 61 p.
- Rogers, G., and H. Dragert (2003), Episodic tremor and slip in Cascadia subduction zone: The chatter of silent slip, *Science*, **300**, 1942–1943.
- Rubinstein, J. L., J. E. Vidale, J. Gomberg, P. Bodin, K. C. Creager and S. Malone (2007), Non-Volcanic Tremor Driven by Large Transient Shear Stresses, *Nature*, **448**, 579–582.
- Rubinstein, J. L., M. La Rocca, J. E. Vidale, K. C. Creager, and A. G. Wech (2008), Tidal Modulation of Non-Volcanic Tremor, *Science*, **319**, 186–189.
- Rubinstein, J. L., D. R. Shelly, and W. L. Ellsworth (2010), Non-volcanic tremor: A window into the roots of fault zones, in *New Frontiers of Solid Earth Sciences*, edited by S. Cloetingh and J. Negendank, pp. 287–314, Springer, Netherlands, doi:10.1007/98790481273758.
- Satake, K., K. Shimazaki, Y. Tsuji, and K. Ueda (1996), Time and size of a giant earthquake in Cascadia inferred from Japanese tsunami records of January 1700, *Nature*, **379**, 246–249, doi:10.1038/379246a0.
- Shelly, D. R., G. C. Beroza, S. Ide, and S. Nakamura (2006), Low-frequency earthquakes in Shikoku, Japan and their relationship to episodic tremor and slip, *Nature*, **442**, 188–191, doi:10.1038/nature04931.
- Wald, D. J., V. Quitoriano, T. H. Heaton, and H. Kanamori (1999), Relationships between Peak Ground Acceleration, Peak Ground Velocity, and Modified Mercalli Intensity in California, *Earthq. Spectra*, **15**(3), 557–564.
- Wech, A. G., and K. C. Creager (2008), Automated detection and location of Cascadia tremor, *Geophys. Res. Lett.*, **35**, L20302, doi:10.1029/2008GL035458.